

Water resource and ecotone transformation in coastal ecosystems

Joseph Park^{a,b,*}, Jed Redwine^{a,c}, Troy Hill^{a,b}, Kevin Kotun^d

^a*Department of Interior South Florida Natural Resources Center*

^b*Physical Resources*

^c*Science Communication*

^d*U.S. Geological Survey*

Abstract

Mangrove marshes are a significant global ecosystem, finely-tuned to contemporary sea level. As sea level rises the mangrove-to-freshwater ecotone reflects underlying groundwater salinity, and when adjacent to populated areas can indicate the transformation of freshwater resources into saltwater unsuitable for consumption or agriculture. Hydrological numerical models can predict this dynamic given sufficient environmental detail, however, detailed data is often lacking. Alternatively, agent-based models can predict landscape vegetation changes and the associated fresh-to-saline water transformation. We apply such a model to the southern tip of the Florida peninsula at the nexus of a metropolis and World Heritage wildlife preserve: the Florida Everglades, to predict ecotone dynamics and aquifer water resources in response to warming climate and rising sea level. The model is based on species-specific behaviors for freshwater grasses and salt-tolerant red mangroves with relevance to global mangrove ecosystems.

Keywords: Freshwater Resource, Mangrove Ecotone, Sea level rise

*Corresponding author

Email address: Joseph_Park@nps.gov (Joseph Park)

¹ **1. Introduction**

² As climate warms and sea level rises, low-lying coastal ecosystems are
³ among the first to transform with potential for large shifts in ecotones and
⁴ associated ecosystem services such as sustenance of freshwater resources.
⁵ These coastal ecotone dynamics reflect landscape changes from the adapta-
⁶ tion of terrestrial, estuarine and marine ecosystems in response to perpetual
⁷ and nonstationary environmental dynamics, and are expressed through a
⁸ web of complex interactions and feedbacks between biota and environment.
⁹ Given the inherent nonlinearity and interdependence in these dynamics, one
¹⁰ would expect that linear systems analysis may provide unsatisfying results
¹¹ (DeAngelis and Yurek, 2015). As noted by Jiang et al. (2016): “While
¹² habitat transitions can be abrupt, modeling the specific drivers of abrupt
¹³ change between halophytic and glycophytic vegetation is not a simple task.
¹⁴ Correlative studies, which dominate the literature, are unlikely to establish
¹⁵ ultimate causation for habitat shifts, and do not generate strong predictive
¹⁶ capacity for coastal land managers”.

¹⁷ Traditional methods to assess these impacts rely on equation-based mod-
¹⁸ els where physical and biological responses are specified with mathematical
¹⁹ expressions and/or probabilistic descriptions and interactions (Jorgensen,
²⁰ 1996). Such numerical models have been instrumental in the advancement
²¹ of our knowledge of coastal systems, however, the expression of emergent
²² behaviors predicated on nonlinear feedbacks can be problematic in the im-
²³ plementation of equation-based models.

²⁴ Specific to the nexus of eco-hydrological models, Sivapalan (2018) noted
²⁵ difficulties in accurately quantifying the spatial heterogeneity needed to in-
²⁶ form equation-based models, thereby complicating the expression of closure

27 relations at scales of interest. Further, he suggested “instead of specifying
28 exact details of the heterogeneity in our models, we can replace it (without
29 loss of information) with the ecosystem function that they perform.” This
30 perspective aligns with the Earth systems science approach (NASA, 1986)
31 relying on integrative co-evolutionary interactions *in-lieu* of a physical, re-
32 ductionist approach.

33 One such alternative is agent-based modeling, where behaviors and feed-
34 backs at the core of the model naturally accommodate nonlinearity and
35 emergence (Grimm, 2005). Here, we assess coastal ecotone dynamics with
36 an agent-based model, relying on vegetative transformations in response
37 to sea level driven porewater salinity as a marker for groundwater changes
38 from fresh to saline. Quantification of these changes, both the landscape
39 transformation from freshwater dominated marshes to saltwater dominated
40 estuaries, and the associated changes in freshwater resources are fundamen-
41 tal to the future of inhabited and natural coastal ecosystems.

42 As an exemplar, we consider the southern tip of the Florida peninsula
43 which is home to both a large metropolitan area and the Everglades (fig-
44 ure 1). The relationship is symbiotic as the Everglades protects and sustains
45 freshwater resources for the natural and urban communities, while concerned
46 citizens and governments are dedicated to preservation and protection of its
47 natural resources. Not only are the Everglades home to spacious freshwater
48 marshes and hardwood hammocks, it includes the largest contiguous fresh-
49 to-saltwater mangrove ecosystem in North America. Such coastal freshwa-
50 ter/mangrove marsh ecosystems are a prominent feature around the globe,
51 with importance as atmospheric carbon sinks, proliferant marine nurseries,
52 and bellwethers of coastal transformation.

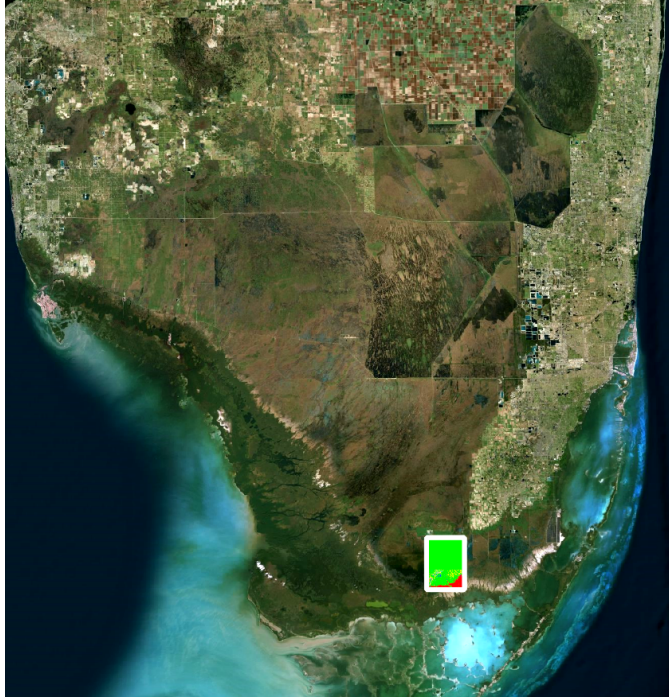


Figure 1: Southern Florida. The east coast is a metropolis of 6.7 million with the South-Dade agricultural area along the southern and western edges. The south central and southwest areas contain the Everglades and Big Cypress National Preserve. The north central area is agricultural and rural. The model domain is shown by the box in the lower center with dimensions 10.2 km x 14.1 km. Dimensions of the overall image are 180 km x 190 km.

53 **2. Materials and methods**

54 *2.1. Analysis Domain and Data*

55 We estimate the change in vegetation coverage and aquifer freshwater
56 volume under a 14,382 hectare model domain spanning a mangrove/freshwater
57 ecotone from 2015 through 2100 in response to a low and high sea level rise
58 trajectory. Figure 2 shows the model domain with a false color overlay of
59 vegetation in 2015 along the southern peninsula.

60 Data inputs consist of landscape vegetation coverage obtained from a
61 synthesis of field observations and aerial photography (Ruiz et al., 2017),
62 marsh water levels from the Everglades Depth Estimation Network (EDEN)
63 (USGS, 2015), land surface elevations (Fennema et al., 2015), and sea level
64 rise trajectories (Park et al., 2017). Model details are described below, with
65 additional information in the Appendix.

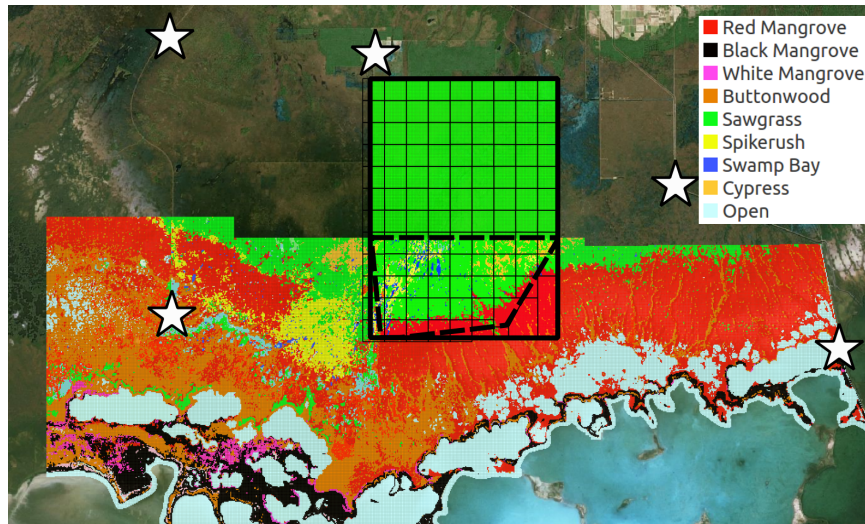


Figure 2: Southern coastal Everglades false color vegetation map. Dashed polygon shows the calibration model domain, rectangle, the future projection domain. The grid defines cells where distinct hydrologic timeseries are applied. Stars indicate locations of wells to estimate aquifer thickness.

66 *2.2. Model Design*

67 Agent-based modeling can be viewed as an evolution of cellular au-
68 tomata (Schiff, 2011), finding good success in the analysis of ecosystem
69 complexity and interactions (Grimm, 2005). Agent-based models consist
70 of dynamically interacting agents operating in a decentralized, intercon-
71 nected paradigm accommodating complexity and emergence. NetLogo is

72 a programmable modeling environment designed to simulate complex phe-
73 nomena in an agent-based framework (Wilensky, 1999), and is the modeling
74 platform we employ.

75 NetLogo distinguishes four types of agents: Patches, Turtles, Links, and
76 Observers. Patches represent the world in a grid of cells. Turtles represent
77 agents that operate in the world, interacting with patches and each other.
78 Links provide connections between agents. Observers allow interaction be-
79 tween agents within, and external to the model domain. Our model defines
80 agents for the dominant vegetation species (turtles), agents for the landscape
81 cells (patches), and interactions between agents and the environment.

82 NetLogo programs conventionally contain `setup` and `go` procedures, the
83 latter being executed in a loop sequencing through agents. The `setup` pro-
84 cedure loads the timeseries input data, loads GIS shapefiles representing the
85 vegetation map and timeseries mappings, initializes patches with data from
86 the GIS layers, and sprouts turtles on the patches according to the GIS
87 vegetation map species for each cell. The `go` procedure iteratively calls the
88 vegetation agents to assess their vitality, followed by the `propagation` pro-
89 cedure governing species succession in response to environmental feedbacks.

90 2.2.1. Vitality behaviors

91 A typical vegetation agent assesses whether the vegetation on a particu-
92 lar patch has been stressed enough to die. For example, *Cladium jamaicense*
93 (sawgrass) contains assessments of hydroperiod, water depth, and porewa-
94 ter salinity thresholds and durations. Vitality conditions resulting in plant
95 death are listed in table 1. Evaluation of environmental variables `days-wet`
96 and `days-dry` in plant vitality behaviors are randomly modulated with a
97 Gaussian kernel to simulate individual plant tolerances. Specifically, when

Table 1: Vitality behaviors. When the condition variable exceeds the threshold, the plant dies. Thresholds are expressed as the NetLogo model variable name (table A.4).

Species	Condition
Sawgrass	depth > <code>sawgrass-depth-max</code>
Sawgrass	days above salinity threshold > <code>sawgrass-salinity-threshold</code>
Spikerush	depth > <code>spikerush-depth-max</code>
Spikerush	days dry > <code>spikerush-days-dry</code>
Spikerush	days above salinity threshold > <code>spikerush-salinity-threshold</code>
Wax Myrtle	depth > <code>wax-myrtle-depth-max</code>
Wax Myrtle	days wet > <code>wax-myrtle-days-wet</code>
Wax Myrtle	days above salinity threshold > <code>wax-myrtle-salinity-threshold</code>

Table 2: Hydroperiod modulation.

Species	Variable	Min	Max	Modulation
Sawgrass	days-wet	0	365	N(0,15) days
Wax Myrtle	days-wet	0	1000	N(0,15) days
Spikerush	days-dry	0	1000	N(0,10) days

98 a patch hydroperiod is processed, the physically simulated value is shifted
 99 by the number of days according to a normal distribution specified in table
 100 2.

101 *2.2.2. Succession behaviors*

102 The `propagation` procedure queries each patch devoid of live vegeta-
 103 tion, assessing surrounding patches to identify neighboring species. If en-
 104 vironmental conditions are conducive for a neighboring species, the species
 105 can establish on the vacant patch according to a fitness function shown in
 106 figure 3.

107 First, a list of vegetation species on the surrounding patches is obtained.

108 A cumulative fitness score is computed for each species by summing the
 109 individual fitness scores on a per-species basis. The species with highest
 110 cumulative fitness is selected for propagation. However, whether propaga-
 111 tion actually occurs is determined by comparison of the species propagation
 112 success threshold (i.e. `mangrove-success`) against a randomly selected per-
 113 centile of a uniform distribution. Table 3 lists conditions that preclude
 114 succession. If succession fails on a particular timestep, there is no penalty
 115 on following timesteps, the `propagation` is run as usual.

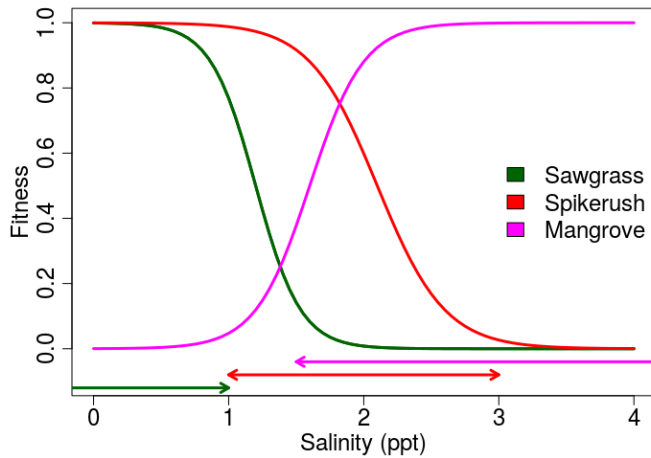


Figure 3: Succession fitness functions for the three dominant species. Horizontal arrows indicate the range of salinity's observed by Ross et al. (2000).

116 2.2.3. Porewater salinity

117 The primary ecotone driver from freshwater to salt-tolerant plants is root
 118 zone porewater salinity, in the model this is driven by the relative elevation of
 119 mean sea level and the vegetation patch. Since there is a coastal ridge along
 120 the northern shore of Florida Bay serving to buffer ocean and estuarine water
 121 from the interior, and, since freshwater in the marsh suppresses subterranean

Table 3: Succession failure conditions.

Species	Condition
Sawgrass	<code>sawgrass-success < uniform percentile</code>
Sawgrass	<code>depth > sawgrass-depth-min</code>
Spikerush	<code>spikerush-success < uniform percentile</code>
Spikerush	<code>days wet < spikerush-days-wet</code>
Mangrove	<code>mangrove-success < uniform percentile</code>
Mangrove	<code>depth > depth-propagule</code>

122 saline water in the root zone as expressed by the Ghyben–Herzburg principle,
 123 there are two model parameters to calibrate these effects: `msl-offset` and
 124 `depth-no-porewater` (see table A.4 and figure A.12).

125 All patches are initialized to porewater salinity of zero, and have a maxi-
 126 mum porewater salinity of 3. This is sufficient since the maximal glycophytic
 127 vegetation tolerance is 2 ppt (table A.4). Patch porewater salinity is then
 128 determined by progressive accumulation of porewater salinity for patches
 129 with elevation below mean sea level.

130 Procedurally, all patches with an elevation below mean sea level mi-
 131 nus the `msl-offset` parameter are selected. If these patches have a fresh
 132 water depth less than `depth-no-porewater`, then their porewater salin-
 133 ity is incremented by 1 ppt. If the fresh water depth is greater than
 134 `depth-no-porewater`, the porewater salinity is reset to zero.

135 *2.3. Vegetation Map*

136 As a component of the Comprehensive Everglades Restoration Plan
 137 (CERP), the Department of Interior conducts an extensive vegetation map-
 138 ping project. The vegetation assessment assigns a landscape characteriza-
 139 tion code, the *vegetation code*, to 50 m x 50 m patches throughout a region.

¹⁴⁰ Vegetation codes derive from a tree of descriptors starting with one of seven
¹⁴¹ overall landscape types, with additional code elements providing increasing
¹⁴² levels of landscape and ecosystem specificity. Since our model is driven by
¹⁴³ species behaviors, we assign the dominant species for each landscape code
¹⁴⁴ to each of the 50 x 50 m patches. Figure 2 shows the southern coastal region
¹⁴⁵ vegetation map in Everglades National Park with false color overlay (Ruiz
¹⁴⁶ et al., 2017).

¹⁴⁷ *2.4. Hydrological Data*

¹⁴⁸ Hydrologic data are informed through the NetLogo `time` extension, with
¹⁴⁹ daily mean water levels provided as timeseries input to patch agents. The
¹⁵⁰ link between timeseries and patches is specified in a GIS layer corresponding
¹⁵¹ to the grid shown in figure 2. Each model grid cell correspond to 3 x 3 grid
¹⁵² blocks from the Everglades Depth Estimation Network (EDEN) (USGS,
¹⁵³ 2015), with the daily water level extracted from the center EDEN cell of the
¹⁵⁴ 3 x 3 block.

¹⁵⁵ EDEN observed data are available from 1990 through 2017. Since the
¹⁵⁶ calibration model period of record is 1973 through 2015, and 2015 through
¹⁵⁷ 2100 for the projection model, data extrapolation is needed. To model data
¹⁵⁸ from 1973 through 1990, we take advantage of strong correlations between
¹⁵⁹ marsh water levels across the model domain ($R^2 = 0.89 \pm 0.09$) and estimate
¹⁶⁰ missing data with linear regressions from each cell to a long term hydrologic
¹⁶¹ station (P-37) in the central Everglades.

¹⁶² Projection model data also leverage strong temporospatial correlations to
¹⁶³ create future projections of stage. These projections are purely probabilistic,
¹⁶⁴ and do not account for climate change or nonstationarity.

¹⁶⁵ First, we compute the mean water level stage of all cells over the obser-

vational record (1990–2017). Second, we compute linear regressions between the timeseries of each grid cell and the mean of all cells ($R^2 = 0.95 \pm 0.05$). Third, we compute empirical distributions for each day of the year (year-day, 1-365) over the observational record from the mean timeseries. Next, the mean timeseries is projected forward in time by sampling from the empirical distribution of the corresponding projected year-day with a Gaussian kernel. That is, for a projected year-day, say the first day of the year, the projected value is sampled from the empirical distribution for the first day of the year at a random percentile selected from a normal distribution. Finally, the linear regressions from the mean to each cell are used to predict timeseries for each cell.

2.5. Sea Level Rise Data

Sea level rise trajectories applied to the future projection model are obtained from Park et al. (2017) corresponding to low (50th percentile) and high (99th percentile) estimates from 2015 through 2100. These estimates are specific to South Florida, and based on a synthesis of tide gauge data, global climate models and expert elicitation, contributions from the Greenland ice sheet, West Antarctic ice sheet, East Antarctic ice sheet, glaciers, thermal expansion, regional ocean dynamics, land water storage and long-term, local, non-climatic factors, such as glacial isostatic adjustment, sediment compaction and tectonics.

As noted in Park et al. (2017), these projections are comprehensive, but do not include components related to a rapid collapse of Greenland and Antarctic ice sheets. Recent observations suggest that such a collapse is underway (Holland et al., 2015; Wouters et al., 2015), thereby we select the median projection as the low, and the 99th percentile as the high. The sea

192 level rise projections and projected marsh water levels are shown in figure
193 4.

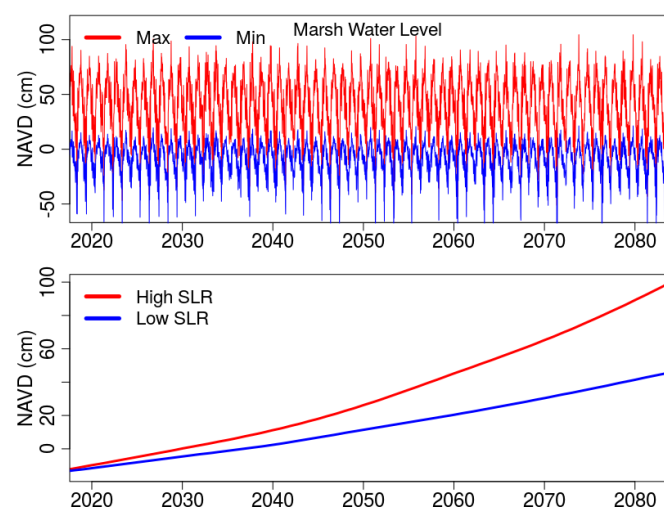


Figure 4: Sea level rise projections (bottom) and projected minimum and maximum marsh water levels (top). Elevations are National Vertical Datum of 1988 (NAVD 88).

194 *2.6. Calibration Model*

195 Calibration of agent thresholds and behaviors is achieved by initializing
196 a model spanning the current mangrove/sawgrass ecotone with vegetation
197 coverage observed in 1973, which at the time was a purely freshwater land-
198 scape as shown in figure 5a). The model domain is a grid of 22,990 patches
199 (209 x 110) covering a spatial domain of 10,450 x 5,500 m. However, only
200 17,680 patches are used according to the extent of the 1973 vegetation map.

201 The model is a four-species model with three freshwater species account-
202 ing for 98% of the initial vegetation (Sawgrass 92%, Spikerush 4%, Wax
203 Myrtle 2%), and Red mangrove as the saline successor. The model is run
204 forward in time from 1973 to 2015 with parameters adjusted to best fit the

205 observed 2015 landscape vegetation (figure 5b). Sea level rise is modeled as
206 a linear function increasing at 3 cm/decade, corresponding to the mean of
207 linear trends at Vaca Key (3.69 mm/yr) and Key West (2.42 mm/yr).

208 Model output is shown in figure 5c. Model parameters are listed in the
209 Appendix (table A.4), model code and data are available in the data archive.

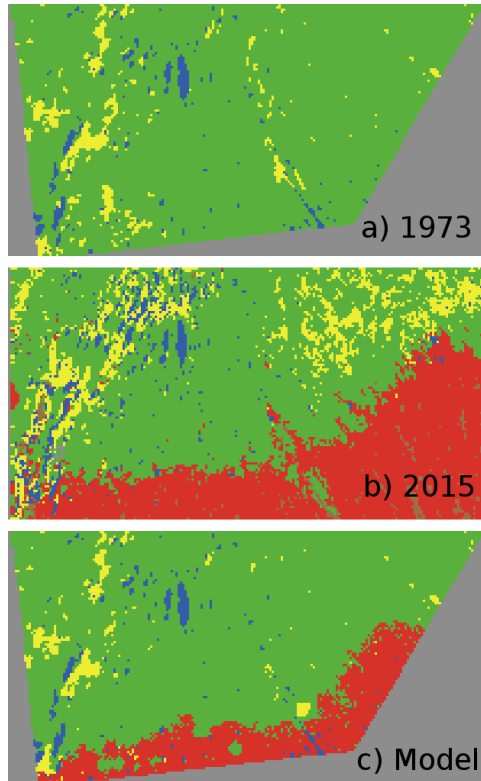


Figure 5: a) Initial vegetation, 1973. b) Final vegetation, 2015. c) Calibration model output at 2015.

210 *2.7. Projection Model*

211 The projection model is a spatial expansion of the calibration model with
212 vegetation initialized from the 2015 vegetation map where available, and

213 with timeseries of marsh stage and sea levels projected from 2015 to 2100.
214 The spatial domain is expanded by 8.6 km to the North and initialized with
215 sawgrass since there is not a vegetation map in this region. The resultant
216 model domain covers 14,382 hectare in a grid of 57,528 patches (204 x 282)
217 10.2 km wide by 14.1 km tall along the fresh to saline ecotone near Taylor
218 Slough, Everglades National Park (figure 2).

219 The model uses parameters determined by the calibration model (table
220 A.4), with the addition of one parameter: `msl-open-depth` and three vege-
221 tation species, Cypress, Swamp Bay and Buttonwood. The `msl-open-depth`
222 defines a patch depth that when exceeded by mean sea level converts the
223 patch from terrestrial to marine/estuarine. It is set to 70 cm corresponding
224 to maximal freshwater depths.

225 3. Results

226 Predicted landscape transformations under low and high sea level rise
227 trajectories are shown in figures 6 and 7 respectively. Under the low sea level
228 rise projection the landscape is relatively unchanged through 2050, with the
229 emergence of a mangrove stand in the south-central model domain. By 2060,
230 the mangrove stand has expanded, and by 2070 it has nearly engulfed the
231 slightly elevated ridge running from the south central of the domain to the
232 northeast. By 2080 the majority of the landscape seaward of the porewater
233 salinity interface has transformed to mangroves, with the emergence of an
234 open water area in the southwest corner of the domain.

235 In response to the high sea level rise trajectory, significant change is not
236 forecast through 2040, with the emergence of the south-central mangrove
237 stand by 2050. The ensuing decade is forecast to support the rapid coloniza-

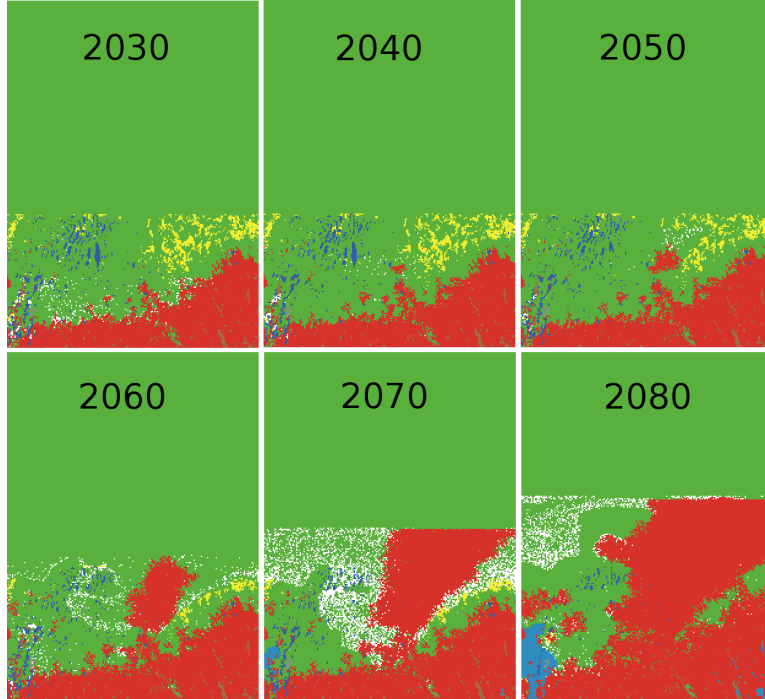


Figure 6: Projected vegetation transformation in response to a low sea level rise trajectory. Vegetation colors correspond to the legend in figure 2. White indicates a dead patch.

tion of mangroves along the slightly elevated ridge. By 2070, there has been substantial transformation with open water accounting for a major portion of the domain and a new coastline of mangrove swamp. By 2080 the transformation from predominantly freshwater marsh to marine conditions and mangrove swamp is nearly complete.

Quantification of the areal change in landscape dominant species vegetation cover in response to the two sea level rise forcings is shown in figure 8. Under both scenarios the contemporary vegetation distributions remain in equilibrium until 2050, beyond which there is evidence of landscape transformation from freshwater marsh to mangrove marsh and open water.

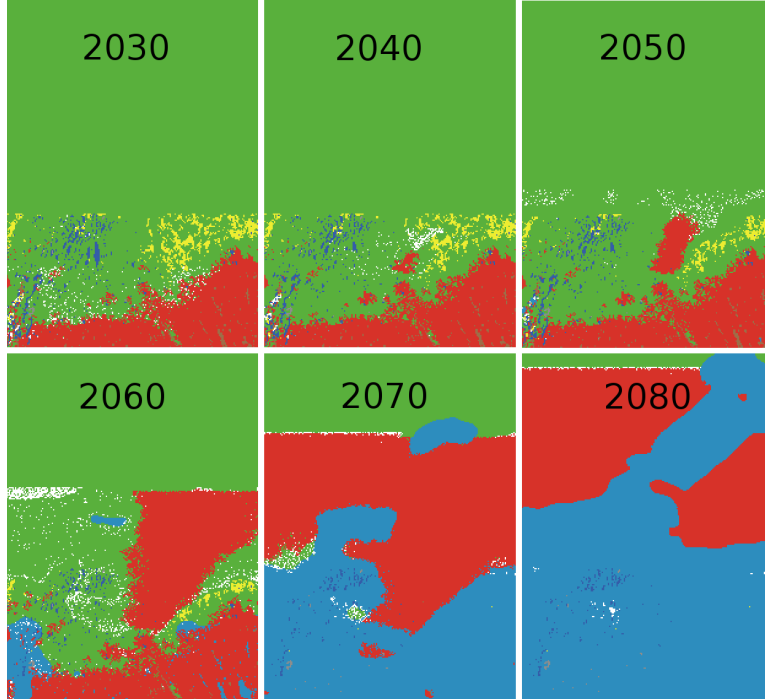


Figure 7: Projected vegetation transformation in response to a high sea level rise trajectory. Vegetation colors correspond to the legend in figure 2. White indicates a dead patch.

The physical mechanism behind freshwater to saline-tolerant vegetation transformation is infiltration of root zone porewater salinity. It is also known that as saline water from rising ocean levels infiltrates landward in the surficial aquifer, it does so from the “bottom-up” since saline water is denser than the freshwater (Dausman and Langevin, 2005). From this, we assume that at a point on the landscape where freshwater vegetation has been displaced that the saline water extends to the base of the surficial aquifer.

Given estimates of the surficial aquifer thickness, which here range from approximately 8 to 12 m (Causaras, 1986), and which are spatially mapped in the model GIS coverage, one can make conservative estimates of the

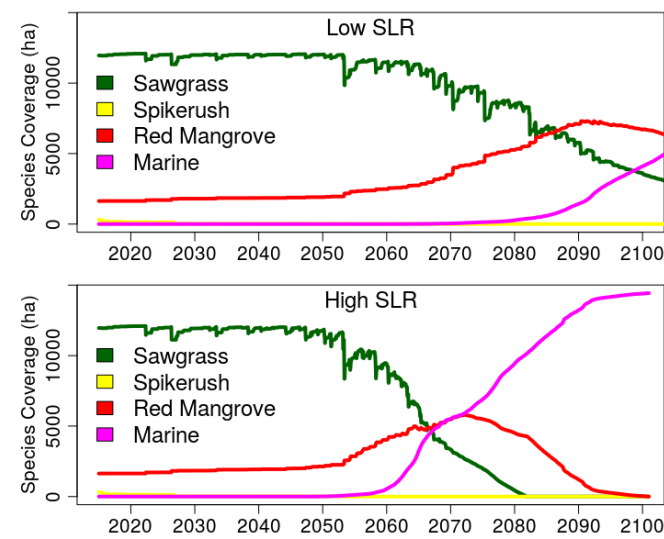


Figure 8: Projection of dominant vegetation coverage and marine (open) area for the low (top) and high (bottom) sea level rise trajectories.

258 freshwater volume replaced by saline water by using the vegetation coverage
 259 as an ecosystem response function. Figure 9 plots estimates of surficial
 260 aquifer volumes under the model domain of fresh and saline water in response
 261 to the two sea level rise trajectories assuming a porewater volume fraction of
 262 0.2 (Dausman and Langevin, 2005). Note that this does not require detailed
 263 estimates of aquifer properties such as hydraulic conductivity.

264 Model results indicate a transformation from current ecological equilib-
 265 rium to saltwater dominated starting at 2050. Dynamics of this transition
 266 from the freshwater biome perspective are presented in figure 10 where devi-
 267 ation of spatially-averaged projected freshwater levels on land are compared
 268 with coverage of the dominant freshwater species from 2050 through 2070.
 269 Here, we find dynamic responses at two timescales. The long-term decline
 270 driven by increasing porewater salinity as ocean levels rise, superimposed

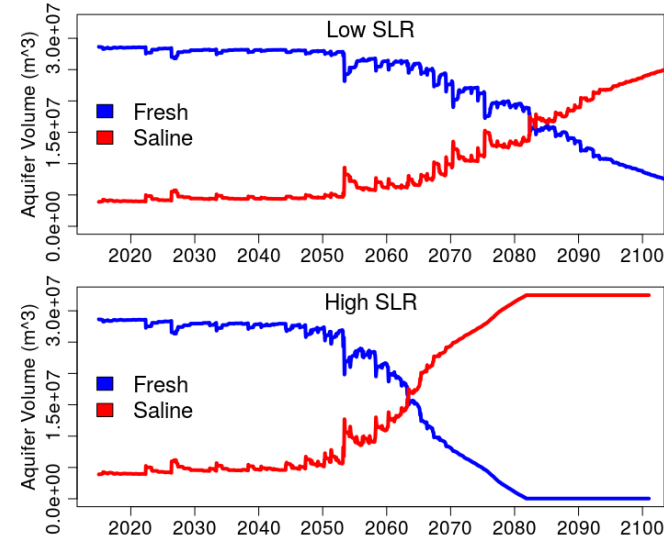


Figure 9: Projection of Fresh and saline water aquifer volumes under the model domain for the low (top) and high (bottom) sea level rise trajectories.

with shorter-term yearly or interannual variations exhibiting species proliferation and recovery, with punctuated events of rapid species decline. The rapid declines appear well-correlated with low freshwater elevation events, consistent with observations that drought and dry conditions are a fundamental stressor of freshwater marsh plants, while recovery is indicated during periods without deep water level recession (2054–2058).

4. Discussion

Following the suggestion of Sivapalan (2018) that complex eco-hydrologic domains can be assessed through ecosystem function expressed on the landscape, and the recognition of Jiang et al. (2016) that linear, correlation-based models may not be ideal for capturing ecotone dynamics, we find that an agent based model provides reasonable and compelling estimates

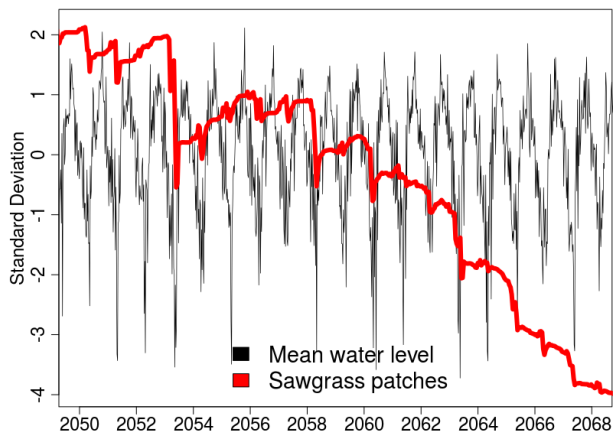


Figure 10: Deviation of spatially-averaged marsh projected water levels compared to scaled sawgrass patch count. Rapid declines in species coverage appear well-correlated with low freshwater elevation events.

for landscape and freshwater resource transformation of coastal marshes in response to sea level rise. The agent based approach relies on specification of interactions between the environment and species competing on the landscape, rather than highly detailed mappings and assumptions of subterranean aquifer geology and environmental forcings such as rainfall and evapotranspiration. If we were not interested in quantifying the aquifer resource transformation, but simply inferring it's areal coverage from the vegetative landscape response, we would not need geologic properties at all.

The model exhibits interspecies competition between fresh and saline tolerant plants, primarily sawgrass (*Cladium jamaicense*) and red mangrove (*Rhizophora mangle*), mediated by root zone porewater salinity determined by elevations of rain-supplied marsh water level, land surface, and sea level. Consistent with known landscape response, elevated porewater salinity denatures freshwater plants during periods of low marsh water level. Open

297 patches are then colonized with fresh or salt tolerant plants depending on
298 environmentally determined fitness functions of surrounding species.

299 Model results predict continued equilibrium between fresh and saltwater
300 species until 2050, after which there is eventual replacement of freshwater
301 species with salt tolerant ones and fresh groundwater with saline groundwa-
302 ter, ultimately transitioning into new marine habitat. Interestingly, initia-
303 tion of the transformation is essentially independent of whether sea levels
304 rise along a low or high trajectory, however, the ensuing transformations
305 are quite different as a function of sea level dynamics. This likely reflects
306 a difference between the low and high sea level rise trajectories of 13 cm
307 between 2020 and 2050, but 70 cm between 2050 and 2100. Under a low sea
308 level rise trajectory the model domain transitions from freshwater resource
309 volume of 28.6 million cubic meters in 2015 to 8.7 million cubic meters in
310 2100, while under a high trajectory the volume decreases to 0 by 2085.

311 The model also predicts that mangrove establishment at the 2050 thresh-
312 old is facilitated along a slightly elevated ridge that runs northeast from the
313 lower central model domain. This elevation difference is no more than 14
314 cm above the surrounding marsh.

315 The anticipated landscape and aquifer transformation horizons of 2050–
316 2070 are consistent with a purely empirical, independent mechanism and
317 analysis by Park et al. (2017a) assessing transformations in water level ex-
318 ceedances along the coastal ridge in Florida Bay, 8.5 km directly south and
319 seaward of the current mangrove–freshwater ecotone. There, the transfor-
320 mation horizon of 2040–2070 is forecast for the coastal ridge to be continually
321 inundated in response to the same sea level rise trajectories.

322 As sea level rises, Florida Bay will expand into the Everglades and
323 South Florida establishing new estuarine and marine habitats replacing fresh

324 groundwater along the coastal ecotone. The model predicts that avoidance
325 of extreme low water events and generally higher marsh stage are keys to
326 prolonging viability of freshwater resources, goals expressed in the Compre-
327 hensive Everglades Restoration Plan (NAS, 2018).

328 Further, as shown in the upper right of figure 2 and lower right of figure
329 1, the South–Dade agricultural areas are less than 10 km from the model
330 domain. This industry employs more than 20,000 people producing more
331 than \$2.7 billion in annual economic impact (Miami Dade Co., 2019), and
332 is predicated on the surficial aquifer as a source of freshwater. Additionally,
333 the Florida Keys Aquaduct Authority extracts potable water for over 70,000
334 residents from a wellfield located less than 5 km from the southern boundary
335 of the agricultural area providing significant concern for saline intrusion
336 (McThenia et al., 2017). Our results suggest that near the end of the century,
337 these areas can start experiencing freshwater resource reduction.

338 Finally, we note that the model is based on species–specific behaviors in
339 response to root zone porewater salinity with freshwater graminoids and red
340 mangroves the dominant cross–ecotone species. Similar coastal ecotones are
341 found around the globe and can be assessed for water resource transforma-
342 tions using these methods.

343 **Appendix A. Appendix**

344 *Appendix A.1. Model Elevation*

345 The interplay between freshwater depths, mean sea level and porewater
346 salinity are largely determined by landscape elevation. Figure A.11 shows
347 the model domain elevation indicating a southwest to northeast channel
348 known locally as Taylor Slough. There is also a small ridge south of Taylor
349 Slough running southwest to northeast. Model simulations suggest that this
350 ridge will provide an initial stand for red mangroves as sea levels rise.

351

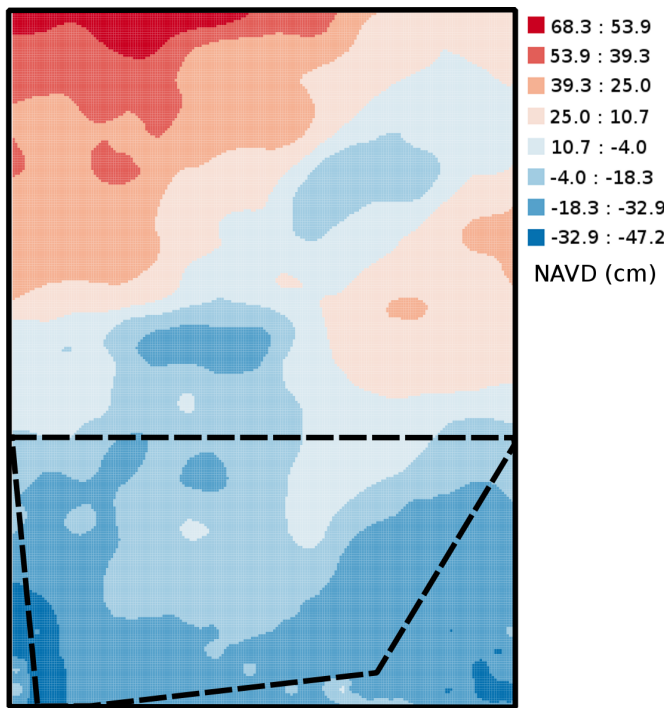


Figure A.11: Elevation map of the model domain. Dashed polygon is the calibration model domain.

352 *Appendix A.2. Calibration Model*

353 Calibration model parameters are shown in table A.4.

Table A.4: Calibration Model Parameters

Parameter	Value	Description
msl-offset	2 cm	Elevation below Mean Sea Level
depth-no-porewater	2 cm	Marsh water depth min for fresh root zone
mangrove-success	33%	Probability of propagation success
depth-propagule	7 cm	Maximum depth for propagule establishment
sawgrass-success	33%	Probability of propagation success
sawgrass-depth-min	20 cm	Maximum depth for propagation
sawgrass-depth-max	180 cm	Maximum depth for survival
sawgrass-salinity-threshold	1	Salinity threshold for survival
sawgrass-salt-days	20	Maximum number of days above threshold
spikerush-success	33%	Probability of propagation success
spikerush-days-wet	730	Hydroperiod for propagation
spikerush-depth-max	80 cm	Maximum depth for survival
spikerush-days-dry	170 cm	Maximum days dry for survival
spikerush-salinity-threshold	2	Salinity threshold for survival
spikerush-salt-days	20	Maximum number of days above threshold
wax-myrtle-depth-max	180 cm	Maximum depth for survival
wax-myrtle-days-wet	370	Maximum hydroperiod for survival

354 Figure A.12 plots model calibration fit in response to `msl-offset` and
355 `depth-no-porewater` finding optimal values of 2 cm for both parameters.
356 Fit is defined as the percentage of model patches that correspond to the
357 2015 observed vegetation at the end of the model run.

358

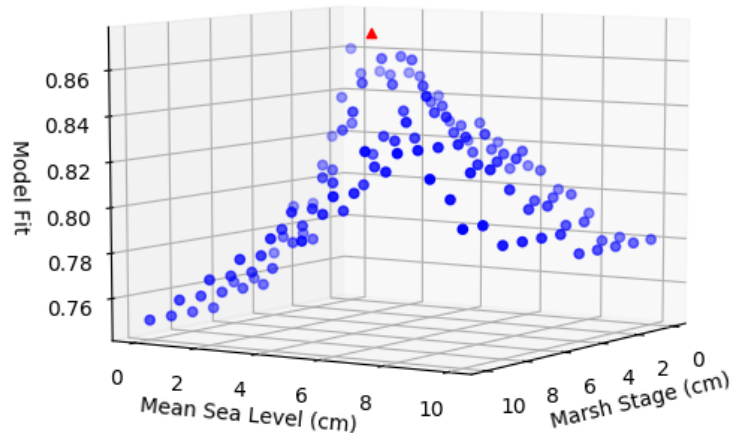


Figure A.12: Model fit as a function of mean sea level offset and marsh stage offset that control porewater salinity.

359 The NetLogo user interface for the calibration model is shown in figure
 360 A.13.

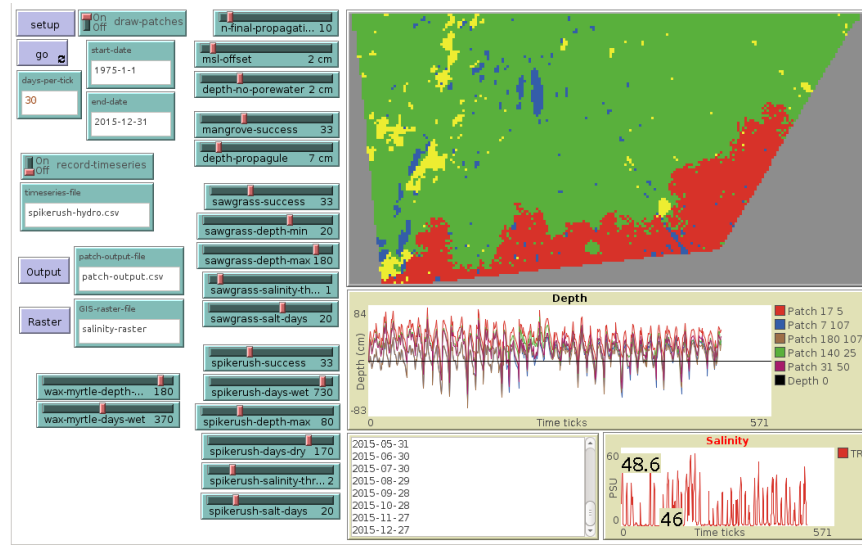


Figure A.13: NetLogo model user interface for the calibration model.

361 *Appendix A.3. Projection Model*

362 The projection model uses the same parameters as the Calibration model
 363 (table A.4), with three additional species. The initial species composition is
 364 shown in table A.5. The NetLogo user interface for the projection model is
 365 shown in figure A.14.

366

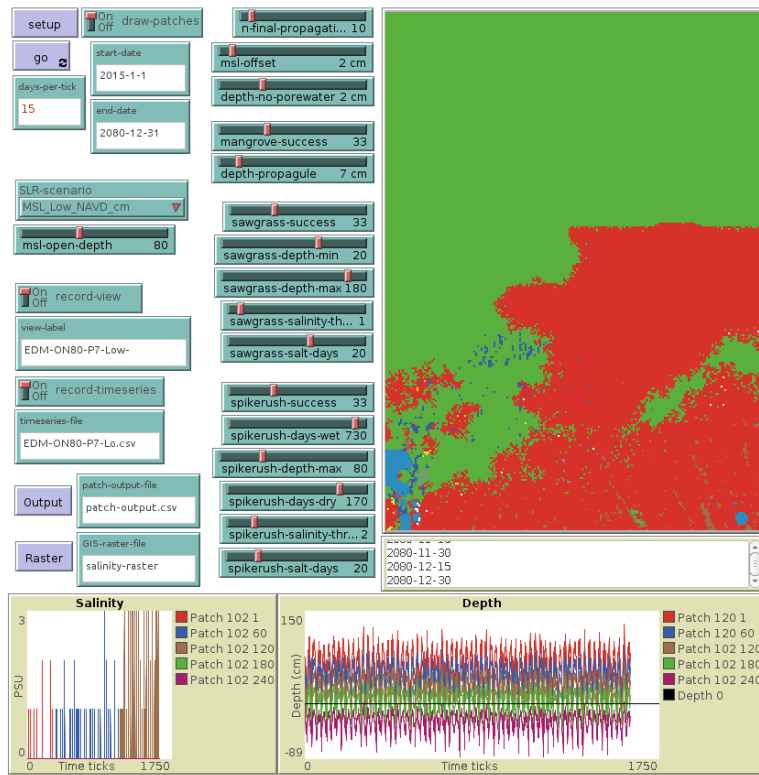


Figure A.14: NetLogo model user interface for the projection model.

Table A.5: Initial species of the projection model.

Species	Count	Percent
Sawgrass	47835	83.1
Red Mangrove	6523	11.3
Spikerush	1258	2.1
Cypress	1070	1.8
Swamp Bay	671	1.1
Buttonwood	395	0.6

367 *Appendix A.4. Aquifer Volume Fit*

368 A generalized logistic function $V = V_0 + \frac{V_{max}}{1+exp(-a(x-x_0))}$ is fit to the
 369 aquifer volume estimates with a Nelder-Mead optimization (Nelder and
 370 Mead, 1965) as shown in figure A.15 and table A.6.

371

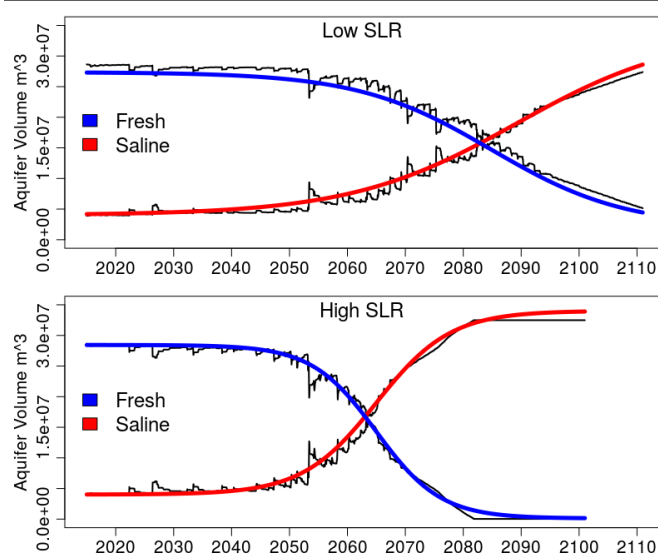


Figure A.15: Generalized logistic function fits to the estimated aquifer water volumes.

Table A.6: Best fit parameters for generalized logistic function $V = V_0 + \frac{V_{max}}{1+exp(-a(x-x_0))}$ fit to estimated aquifer water volumes.

SLR	Water	a	V_{max}	V_0	x_0
Low	Salt	0.0001907	29999684	4011159	2089-04-04
Low	Fresh	-0.0002369	25303766	2051779	2084-11-14
High	Salt	0.0004285	29999999	4010603	2064-12-31
High	Fresh	-0.0004918	28322591	117512	2064-12-31

372 *Appendix A.5. Aquifer Geological Data*

373 Aquifer thickness is inferred from United States Geological Service wells

374 and geologic cross-sections shown in figure A.16.

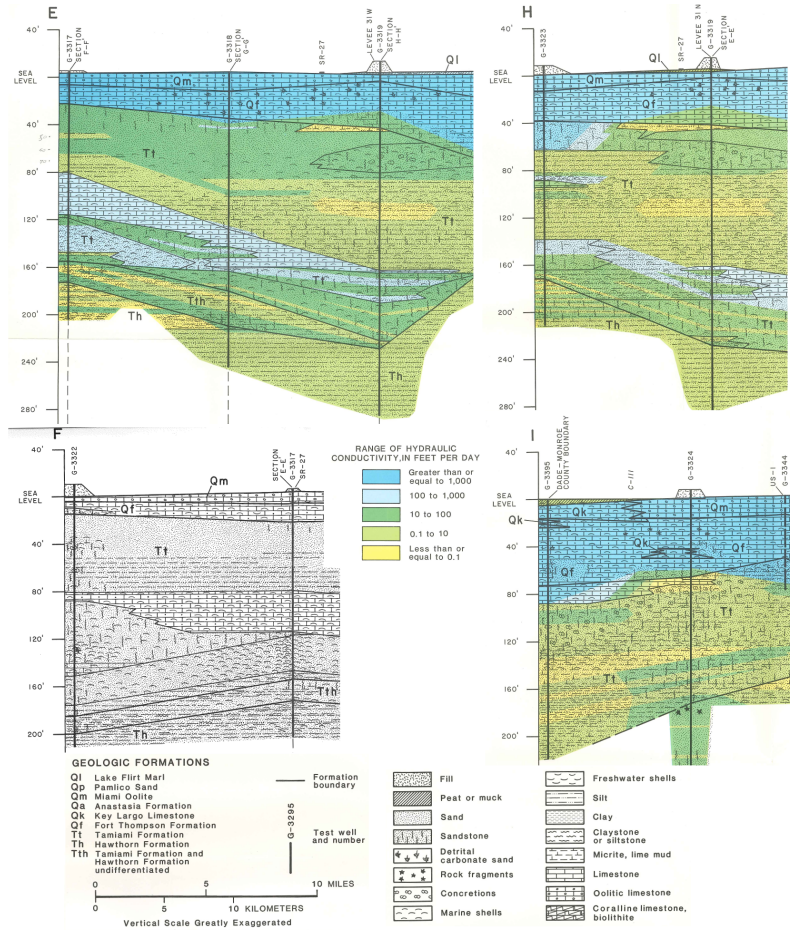


Figure A.16: Geologic cross sections from United States Geological Service wells
(Causaras, 1986)

375 **References**

- 376 Causaras, C. A. (1986). Geology of the surficial aquifer system, Dade County,
377 Florida, Water-Resources Investigations Report 86-4126, U.S. Geological
378 Survey, doi:10.3133/wri864126.
- 379 Dausman, A., and Langevin, C.D., (2005). Movement of the saltwater in-
380 terface in the surficial aquifer system in response to hydrologic stresses
381 and water-management practices, Broward County, Florida. USGS Sci-
382 entific Investigations Report 2004-5256. [http://pubs.usgs.gov/sir/](http://pubs.usgs.gov/sir/2004/5256/)
383 2004/5256/
- 384 DeAngelis D.L., Yurek S. (2015). Equation-free modeling unravels the
385 behavior of complex ecological systems. PNAS 112 (13) 3856-3857,
386 doi:10.1073/pnas.1503154112.
- 387 Fennema, R., James, F., Bhatt, T., Mullins, T., Alarcon, C. (2015). EVER
388 Elevation (version 1): A multi-sourced Digital Elevation Model for Ever-
389 glades National Park. National Park Service, Everglades National Park,
390 950 N Krome Ave. Homestead FL, USA, July 10, 2015.
- 391 Grimm V., Railsback S.F. (2005). *Individual-Based Modeling and Ecology*,
392 Princeton Univ Press, Princeton, NJ.
- 393 Holland, P. R., A. Brisbourne, H. F. J. Corr, D. McGrath, K. Purdon, J.
394 Paden, H. A. Fricker, F. S. Paolo, and A. H. Fleming (2015). Oceanic and
395 atmospheric forcing of Larsen C Ice-Shelf thinning, The Cryosurgery, 9,
396 1005-1024, doi:10.5194/tc-9-1005-2015.
- 397 Jiang J, DeAngelis D., Teh S., Krauss K., Wang H., Lie H., Smith T.,
398 Koh H., (2016). Defining the next generation modeling of coastal ecotone

- 399 dynamics in response to global change. Ecological Modelling, 326, 24 April
400 2016, 168-176. <https://doi.org/10.1016/j.ecolmodel.2015.04.013>.
- 401 Jrgensen, S. E. (1996). *Handbook of environmental and ecological modeling*.
402 CRC Press. Boca Raton, FL. 688 p., ISBN 978-1-56670-202-7.
- 403 Miami–Dade County Agriculture, (2019). <https://www.miamidade.gov/business/agriculture.asp>. Accessed January 3, 2019.
- 404
- 405 McThenia A., Martin W., and J Reynolds, (2017). Rising Tides
406 and Sinking Brines: Managing the Threat of Salt Water In-
407 trusion. Florida Water Resources Journal, August, 32–38.
408 <https://fkaa.blob.core.windows.net/linkdocs/Managing%20the%20Threat%20of%20Salt%20Water%20Intrusion.pdf>.
- 409
- 410 National Academies of Sciences, Engineering, and Medicine (2018). Progress
411 Toward Restoring the Everglades: The Seventh Biennial Review - 2018.
412 Washington, DC: The National Academies Press. 210 p. ISBN: 978-0-309-
413 47978-3 doi:10.17226/25198.
- 414 NASA Advisory Council. Earth System Sciences Committee. (1986).
415 *Earth system science overview: a program for global change*. Wash-
416 ington, D.C.: National Aeronautics and Space Administration, 50 p.,
417 doi:10.17226/19210.
- 418 Nelder, J. A. and Mead, R. (1965). A simplex algorithm for function mini-
419 mization. Computer Journal, 7, 308313. doi:10.1093/comjnl/7.4.308.
- 420 Park, J., Stabenau E., and K. Kotun (2017). Sea-level rise and in-
421 undation scenarios for national parks in South Florida, Park Sci-

- 422 ence 33(1):63-73. https://www.nps.gov/articles/parkscience33-1_63-73_park_et_el_3860.htm.
- 424 Park J., Stabenau E., Redwine J., Kotun K. (2017). South Florida's En-
425 croachment of the Sea and Environmental Transformation over the 21st
426 Century, J. Mar. Sci. Eng., 5(3), 31, doi:10.3390/jmse50300312017.
- 427 Ross M., Meeder J., Sah J., Ruiz P. and G. Telesnicki (2000). The South-
428 east Saline Everglades Revisited: 50 Years of Coastal Vegetation Change.
429 Journal of Vegetation Science, 11(1), 101-112. <http://www.jstor.org/stable/3236781>.
- 431 Ruiz P., Giannini H., Prats M., Perry C., Foguer M., Garcia A., Sham-
432 blin R., Whelan K., Hernandez M. (2017). The Everglades National
433 Park and Big Cypress National Preserve Vegetation Mapping Project, In-
434 terim Report Southeast Saline Everglades (Region 2). Everglades National
435 Park Natural Resource Report NPS/SFCN/NRR2017/1494. August 2017.
436 <https://irma.nps.gov/DataStore/DownloadFile/583479>.
- 437 Schiff, Joel L. *Cellular Automata: A Discrete View of the World*. Wiley &
438 Sons, Inc. ISBN 9781118030639. (2011).
- 439 Sivapalan, M. (2018). From engineering hydrology to Earth system science:
440 milestones in the transformation of hydrologic science, Hydrol. Earth Syst.
441 Sci., 22, 1665-1693, doi:10.5194/hess-22-1665-2018.
- 442 Telis P.A., Zhixiao X., Zhongwei L., Yingru L, and Conrads P. (2015). The
443 Everglades Depth Estimation Network (EDEN) Surface-Water Model,
444 Version 2: U.S. Geological Survey Scientific Investigations Report 2014-
445 5209, 42 p., doi 10.3133/sir20145209.

⁴⁴⁶ Wilensky, U. (1999). NetLogo. Center for Connected Learning and
⁴⁴⁷ Computer-Based Modeling, Northwestern University, Evanston, IL. <http://ccl.northwestern.edu/netlogo/>.

⁴⁴⁹ Wouters B., A. Martin-Español, V. Helm, T. Flament, J. M. van Wessem, S.
⁴⁵⁰ R. M. Ligtenberg, M. R. van den Broeke and J. L. Bamber (2015). Dy-
⁴⁵¹ namic thinning of glaciers on the Southern Antarctic Peninsula, Science,
⁴⁵² 348 (6237) 899-903, doi:10.1126/science.aaa5727.